

## Microstructure of Amphiphilic Monodendrons at the Air–Water Interface

Kirsten L. Genson,<sup>†</sup> David Vaknin,<sup>‡</sup> Ovette Villacencio,<sup>§</sup> Dominic V. McGrath,<sup>§</sup> and Vladimir V. Tsukruk\*,<sup>†</sup>

*Department of Materials Science and Engineering, Iowa State University, Ames, Iowa 50011, Ames Laboratory and Department of Physics and Astronomy, Iowa State University, Ames, Iowa 50011, and Department of Chemistry, University of Arizona, P.O. Box 210041, Tucson, Arizona 85721*

Received: June 5, 2002; In Final Form: September 5, 2002

Grazing incident X-ray diffraction and X-ray reflectivity have been performed on Langmuir monolayers of low generation monodendrons containing a crown-ether polar group, azobenzene spacer, and varying number of peripheral alkyl chains of 1, 2, 4, and 8. We observe that the cross-sectional mismatch between the bulky polar head and the alkyl tails has a profound effect on the local ordering of the alkyl tails. It is found that the alkyl chains in a single-tail molecule are significantly tilted away from the surface normal. The tilt is eliminated in molecules with two or more alkyl chains where the cross-sectional mismatch is in favor of the peripheral tails. The molecule with one tail possesses a supercell orthorhombic packing caused by structural nonequivalency on the neighboring tails. The two- and four-tail molecules form a mixed structure best described by a quasi-hexagonal unit cell, and the eight-tail molecule forms a more stable hexagonal unit cell. Peripheral tails for these molecules are in standing-off orientation. We suggest that the steric constraints cause lower correlations and a staggered packing structure of monolayers from the eight-tail molecule. We suggest that branching alkyl tails off the same phenyl ring and the presence of the phenyl rings in the vicinity of the branching are limiting factors on the chain packing at the air–water interface in monodendrons with multiple peripheral tails. We conclude that a significant portion of the molecules is submerged in the water subphase and possesses a “kink” shape.

### 1. Introduction

Dendrimers have become of great interest in recent years because of their ability to organize into supramolecular structures of various shapes and sizes.<sup>1,2</sup> The structure of monodendrons with appropriate amphiphilic balance between hydrophilic cores and hydrophobic shells allows for the ordered organization of the molecules at interfaces and surfaces in the form of self-assembled or Langmuir monolayers. By varying the chemical architecture of the branches and peripheral tails the interfacial behavior and microstructure can be dramatically altered. The stability of the dendrimer monolayers and their internal ordering are directly related to the molecular dimensions of the hydrophobic and hydrophilic parts of the molecules.<sup>3</sup>

X-ray and neutron studies of Langmuir layers have been extensively used for monolayers of simple amphiphilic molecules for decades.<sup>4</sup> Recently, these techniques have been exploited to study the structure of monolayers of complex dendritic molecular architectures at the air/water interface.<sup>3,5</sup> It has been shown that simple amphiphilic molecules with conventional polar heads (hydroxyl, carboxyl) and long alkyl tails possess large angle tilts from the surface normal ( $18^\circ$  to  $40^\circ$ ) at very low surface pressures when the available surface area per molecule far exceeds the  $19\text{--}20 \text{ \AA}^2$  required for dense packing of alkyl chains.<sup>6</sup> However, the degree of tilt has been

closely linked to the surface pressure of the Langmuir layer.<sup>7,8</sup> Chain tilt within a Langmuir monolayer is reduced or eliminated completely as the pressure is increased and the layer transforms from the low-pressure phase region to the high-pressure phase region.<sup>9</sup> The small tilt ( $5^\circ\text{--}10^\circ$ ) still observed at high surface pressure is caused by the minor mismatch between the molecular dimension of the polar head and the alkyl tail and dense packing of trans chains with collective chain shift.

Little focus has been directed at the intralayer packing of alkyl tails when a significant cross-sectional mismatch occurs between the headgroup of the molecule and/or when multiple tails are attached to the same focal point. Bulky crown heads attached to hydrophobic tails have been used in several cases.<sup>5,10</sup> A phase transformation has been observed at higher pressures and was associated with a structural transition from planar to folded conformation of side chains.<sup>10</sup> Changing the orientation of crown heads from edge-on to face-on at the air–water interface has been reported for multi-chain molecules. Bulky crown-ether polar heads have been attached as the focal group to monodendron molecules, and Langmuir monolayers have been studied.<sup>11</sup> It has been suggested that molecules lie essentially flat at low surface pressures but form stable monolayers with standing chains at high surface pressures. The authors focused on higher generation molecules where the densely packed region contained the multiple tails of the molecule and discussed data derived from electron density along the surface normal.

Our previous work on monodendrons with bulky crown heads has been devoted to the effect of the cross-sectional mismatch on the properties of Langmuir and Langmuir–Blodgett layers.<sup>12,13</sup> We demonstrated that loose packing of the focal

\* Author to whom correspondence should be addressed. E-mail: Vladimir@iastate.edu.

<sup>†</sup> Department of Materials Science and Engineering, Iowa State University.

<sup>‡</sup> Ames Laboratory and Department of Physics and Astronomy, Iowa State University.

<sup>§</sup> Department of Chemistry, University of Arizona.

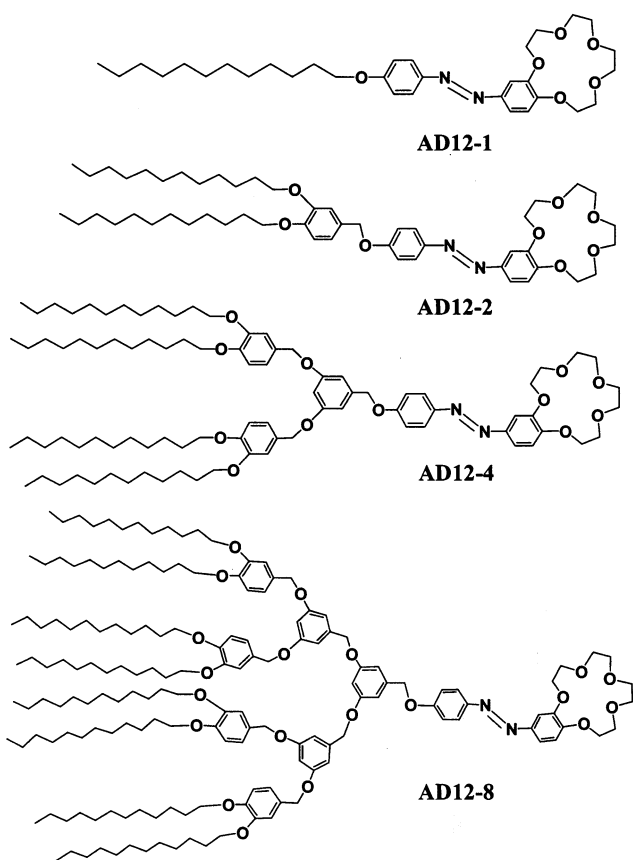


**Figure 1.** Dendrimer compounds studied. AD12-*N* corresponds to the compound with *N* peripheral tails.

azobenzene groups resulted in their reversible photoresponsive behavior. Recently, X-ray reflectivity and X-ray grazing incident diffraction (XGID) have been performed on Langmuir layers of such molecules.<sup>14</sup> We observed that for single-tailed molecules in a monolayer form, the alkyl tails tilt significantly to account for the large cross-sectional mismatch and form double-supercell lateral packing with orthorhombic symmetry. In the present study, we focus on the expansion of that study considering the one, two, four, and eight-tailed azobenzene monodendron compounds.

## 2. Experimental Section

The **AD12-N** ( $N$  represents the number of tails per molecule) series of molecules is presented in Figure 1. All four molecules have a crown-ether head attached to a photochromic group. The synthesis and general characteristics were previously described elsewhere.<sup>15</sup> Monomolecular films were prepared by the Langmuir techniques on a temperature-controlled, Teflon trough. During the synchrotron experiments, the trough was placed in a helium environment to reduce the background scattering from air and prevent an oxidation reaction that can damage the monolayer. Monolayer preparation for the synchrotron studies is described in detail in a previous publication.<sup>14</sup>

A combination of XGID (in-plane and rod-scans) and X-ray reflectivity measurements was used to characterize the monolayer structure according to the known approach.<sup>16–18</sup> Experiments were conducted on the Ames Laboratory liquid-surface diffractometer at the 6ID beam line at the Advanced Photon Source synchrotron at Argonne National Laboratory. Details regarding X-ray reflectivity and XGID and the experimental setup are described elsewhere.<sup>14,19</sup> A downstream Si double

crystal monochromator was used to select the X-ray beam at the desired energy ( $\lambda = 0.772 \text{ \AA}$ ).

The box model was used to determine the electron densities across the interface and to relate them to the molecular arrangements of the molecular fragments at the interface.<sup>20</sup> The box model consists of slabs of differing thickness and electronic density stacked above the water subphase with known electron density ( $0.33 \text{ e}/\text{\AA}^3$ ). The interfaces are smeared to account for the surface roughness and thermal vibrations. The arrangement of the molecular segments can be determined from the length and electron density of the boxes via direct comparison with molecular models. The reflectivity used to fit the experimental data was calculated from

$$R(Q_z) = R_0(Q_z) e^{-(Q_z \sigma)^2} \quad (1)$$

where the  $R_o(Q_z)$  is the reflectivity from steplike functions and  $\sigma$  is the surface roughness.

Rod scans along the surface normal at the 2D Bragg's reflections were measured to determine the form factor of the diffracting objects. The intensity was quantitatively analyzed along the 2D Bragg reflection rod by using the framework of the distorted wave Born approximation (DWBA).<sup>21</sup>

$$I \propto |t(k_{z_f})|^2 |F(Q_z)|^2 \quad (2)$$

where  $t(k_{z,f})$  is the Fresnel transmission function which gives rise to the enhancement around the critical angle of the scattered beam. The Fresnel transmission function is defined as  $k_{z,f} = k_0 \sin\beta$ , where  $k_0$  is  $2\pi/\lambda$  and  $\beta$  is the angle of the scattered beam with respect to the surface. The alkyl tails were modeled as cylinders of a length  $l$  and a fixed radius equal to the cross-sectional radius of alkyl chains. In simulation of the rod scans, the length and tilt of the tails were varied, and the intensity was adjusted for two tilt directions: one toward nearest neighbors (NN) and the second toward next NN (NNN).<sup>22</sup> The form factor for the tails is given by

$$F(Q_z') = \sin(Q_z' l/2)/(Q_z' l/2)$$

where  $Q_z'$  is defined along the long axis of the tail.

Molecular models were built with a Cerius<sup>2</sup> 3.8 package on a SGI workstation by using the Dreiding 2.21 force field library. Molecular models were treated with a molecular dynamics and a minimization procedure to obtain conformations with minimized energy. The alkyl tails were densely packed using parameters deduced from experimental data to analyze possible steric restrictions and the ability of the molecules to adapt the molecular packing proposed.

### 3. Results and Discussion

## Surface-Pressure versus Molecular Area ( $\pi$ - $A$ isotherm)

**Behavior.** All molecules presented in Figure 1 form stable monolayers at the air–water interface, as was discussed in detail in a previous publication.<sup>12</sup> Upon compression, the surface pressure increases as the molecular area of the monolayer decreases, resembling classic amphiphilic behavior. The cross-sectional area for the crown-ether head in flat-on orientation at the interface is determined to be  $45 \text{ \AA}^2$ . Figure 2 shows the observed surface area per molecule and the calculated cross-sectional area per tail for the four molecules. The molecular area determined from pressure–area isotherms for the one-, two-, four-, and eight-tail compounds is 43, 48, 77, and  $155 \text{ \AA}^2$ , respectively (Figure 2). For one- and two-tail molecules, the observed cross-sectional area per tail is larger than  $20 \text{ \AA}^2$ ,

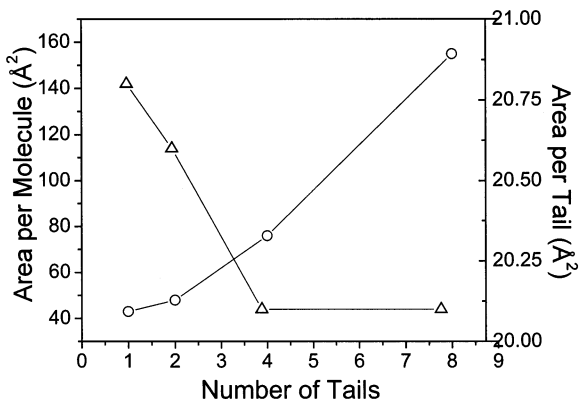


**Figure 2.** Variation of observed cross-sectional area per molecule (circles) and the cross-sectional area per tail (triangles) for the **AD12-1** series.

**TABLE 1: Structural Parameters of the Langmuir Monolayers from Different Dendrimer Compounds<sup>a</sup>**

	stearic acid	AD12-1	AD12-2	AD12-4	AD12-8
d-Spacings, ( $\text{\AA}$ )					
peak 1		6.26	8.62		
peak 2	4.24	4.40	4.71	4.18	4.17
peak 3	4.18	3.94	4.22		
Unit Cell Parameter					
<i>a</i> ( $\text{\AA}$ )	8.36 <sup>a</sup>	7.88	4.87	4.83	4.82
<i>b</i> ( $\text{\AA}$ )	4.83 <sup>a</sup>	5.29			
area per chain ( $\text{\AA}^2$ )	19.7	20.8	20.6	20.1	20.1
chain tilt ( $^\circ$ )	16.5	$\sim 58^\circ$	4°	3°	4°
Correlation Length, ( $\text{\AA}$ )					
peak 1		192			
peak 2	57	165			
peak 3	71	171	35	28	37

<sup>a</sup>The values for stearic acid were taken from Peterson et al.<sup>23</sup>

the typical cross-sectional area of a single alkyl tail.<sup>7</sup> However, for monodendrons with four and eight tails, cross-sectional area per tail decreases to about the expected value (Table 1). As discussed earlier,<sup>12,13</sup> the molecular area of lower generation monodendrons is determined by the crown-ether polar head, while the molecular area of the higher generation is dictated by the alkyl tails.

**X-ray Diffraction Analysis of Intralayer Order.** For the low-pressure region of the  $\pi$ -A isotherm, the **AD12-1** monolayer produces no peaks visible in the diffraction pattern as shown in Figure 3a. Upon reaching the higher-pressure region of the isotherm, three peaks become visible. The peaks are associated with the  $(1, \frac{1}{2})$ ,  $(1, 1)$ , and  $(2, 0)$  peaks of an orthorhombic supercell described in detail in an earlier publication.<sup>14</sup> The *d* spacings of the three peaks are 6.26, 4.40, and 3.94 Å, which correspond to a unit cell of 7.88 by 5.29 Å (Table 1). The mismatch in the cross-sectional area of the crown head and a single alkyl tail allows for the packing of the monolayer on the surface to be dictated by the polar head while allowing the tails to tilt to compensate for the mismatch. Scans obtained under higher reflection angle presented in Figure 3b confirm the tilted orientation of the densely packed tails by the gradual select disappearance of the  $(1, 1)$  peak at a higher reflection angle, as expected for next-next neighbor tilt mode.<sup>22</sup>

Increasing the number of alkyl tails from one to two changes the molecular area determined from the  $\pi$ -A isotherm slightly, but greatly changes the diffraction pattern (Figure 4a). Two well-defined peaks appear for the **AD12-2** monolayer at both low and high pressures. At higher surface pressure, these peaks

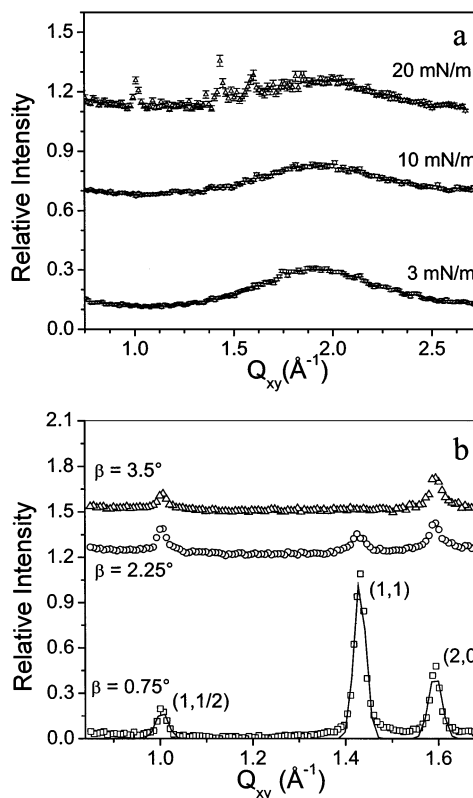


**Figure 3.** Diffraction patterns of **AD12-1** for (a) the whole observed range of  $Q_{xy}$  at three surface pressures, and (b) the high-resolution scans upon increasing the detector away from the horizon ( $\beta$ ); solid lines are Lorentzian fits. The original intensities are offset for clarity.

become more intense and an additional intermediate peak appears. The higher *Q* region appears to have a weak peak that can be refined to a third peak. The *d* spacings of the three peaks on this plot (and for all other compounds) were obtained from high-resolution scans by using data fit with Lorentzian functions. The obtained values were 8.62, 4.71, and 4.22 Å (Table 1). The intensity of first two peaks is too low to be used in the calculation of the unit parameters and could originate from a mixed intramonomolayer structure. Therefore, we indexed only the most intensive peak as the  $(1, 0)$  reflection of the hexagonal lattice with the lattice parameter *a* = 4.87 Å (Figure 4b, Table 1). This unit cell gives the surface area of 20.6 Å<sup>2</sup> per alkyl tail, which is close to that for the first generation (Figure 2). The width of the diffraction peak indicates disordering of the unit cell. The hexagonal structure appears to be an intermediate stage between the previous supercell orthorhombic unit cell of the lower generation and an ordered hexagonal unit cell for higher generation molecules (see below). Figure 4b shows the high-resolution diffraction scans of the **AD12-2** monolayer obtained at different reflection angles. All diffraction peaks disappear upon the slight increase of the reflection angle, leading to the conclusion that the tails are in standing-off orientation for this molecule, unlike the molecule with one tail, **AD12-1**.

The diffraction pattern for the compound with four alkyl tails, **AD12-4**, unlike the two previous compounds, displays only one intensive peak, even at the lowest surface pressure (Figure 5a). The presence of the peak indicates the formation of dense lateral packing of the alkyl tails within the monolayer. The peak position at 1.50 Å<sup>-1</sup> corresponds to 4.18 Å *d* spacing. From the broad single peak, a quasi-hexagonal unit cell was calculated with a 4.83 Å side and 20.1 Å<sup>2</sup> area per chain (Table 1). The broadness and asymmetry of the peak indicates the single peak can be refined into two overlapping peaks shown in Figure 5b.

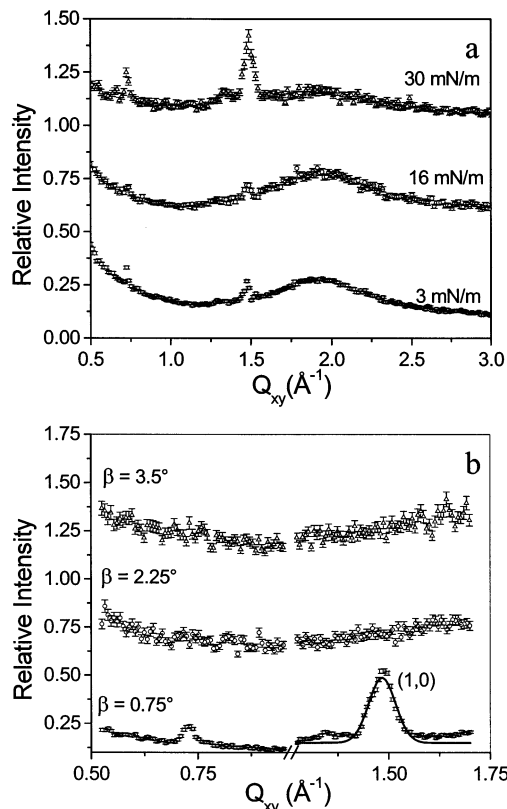


**Figure 4.** Diffraction patterns of **AD12-2** for (a) the whole observed range of  $Q_{xy}$  at three surface pressures, and (b) the high-resolution scans upon increasing the detector away from the horizon ( $\beta$ ); solid lines are Lorentzian fits. The original intensities are offset for clarity.

As with the **AD12-2** monolayer, the diffraction peaks disappear as the  $\beta$  angle is increased (Figure 5b), indicating upright orientation of the alkyl tails similarly to **AD12-2** and in contrast with **AD12-1**.

One sharp peak is present in the diffraction pattern for **AD12-8** at  $Q = 1.50 \text{ \AA}^{-1}$  for all three surface pressures (Figure 6a). The single peak leads to the calculation of a hexagonal unit cell with a length of  $4.82 \text{ \AA}$  and the surface area of  $20.1 \text{ \AA}^2$  per alkyl tail (Table 1). This unit cell is nearly identical to the **AD12-4** unit cell but appears to indicate a more regular hexagonal packing structure with limited short-range ordering rather than the hexagonal structure of the previous two generations. The diffraction peak disappears as the  $\beta$  angle is increased (Figure 6b), indicating tails that are normal to the surface similar to two- and four-tail molecules.

Figure 7 shows the comparison of the diffraction patterns for the highest pressure of all monolayers from the four compounds with different number of alkyl tails. Two diffraction peaks observed in the  $1.4\text{--}1.6 \text{ \AA}^{-1}$  region confirm the formation of the orthorhombic unit cell with parameters shown in Table 1. The molecule with one tail has an additional peak that indicates a supercell packing of the alkyl tails caused by steric limitations imposed by their attachment to the polar head (Figure 8). The necessity to pack bulky polar groups beneath the alkyl sublayer may result in structural nonequivalency on the neighboring tails, causing the effect observed. Simple fatty acids such as stearic acid have been used as comparisons for more complex systems because their chemical structure allows for simple models to describe their packing structures (Figure 8).<sup>7,23</sup> The small cross-sectional mismatch between the carboxyl headgroup and a hydrocarbon chain, generally, causes a slight tilt in the NN direction.<sup>23</sup> At lower and intermediate surface pressures,

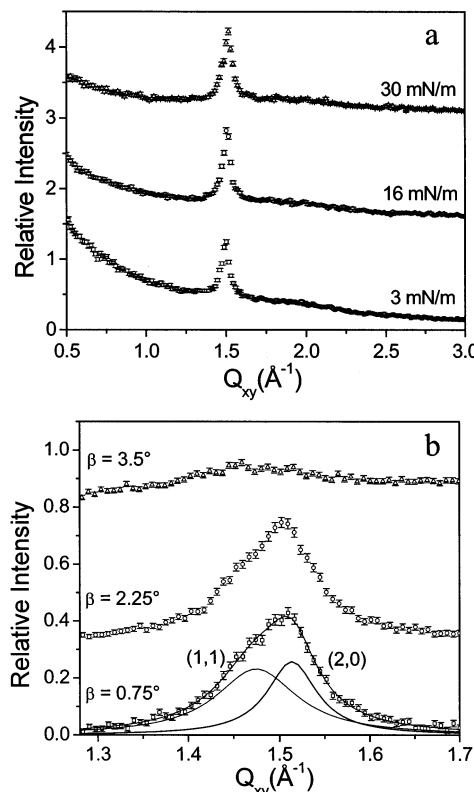


**Figure 5.** Diffraction patterns of **AD12-4** for (a) the whole observed range of  $Q_{xy}$  at three surface pressures, and (b) the high-resolution scans upon increasing the detector away from the horizon ( $\beta$ ); solid lines are Lorentzian fits. The original intensities are offset for clarity.

the tilt angle is in the range of  $15\text{--}30^\circ$ . Peterson et al. calculated the area per tail for stearic acid to be between  $19.5$  and  $20.0 \text{ \AA}^2$  for higher pressures, smaller than the cross-sectional areas calculated for **AD12-1** and **AD12-2** but close to that observed for **AD12-4** and **AD12-8** (Table 1).<sup>23</sup>

The effective cross-sectional area per tail drops when four or more tails are attached to the polar fragment (Table 1, Figure 2). For molecules with multiple chains, the alkyl tails are oriented along the surface normal, unlike the molecule with a single chain with a large tilt of the alkyl tails. For these compounds, the total cross-sectional area of the alkyl tails is much higher than the molecular area of the polar head. Thus, the loosely packed polar heads do not distort the dense packing of the alkyl chain, although the intralayer correlations diminish significantly (Table 1).

Indeed, the correlation lengths calculated for the diffraction peaks for each compound show an interesting trend (Table 1). The molecule with the most ordered (highest correlation length) intralayer packing is **AD12-1**, although the calculated lengths are close to the resolution limit. The correlation length is reduced dramatically for the two-tail compound and is further reduced for the four- and eight-tail compounds. This decrease is obviously caused by the steric conflicts within branched tails. Multiple tails attached to a single core must stagger in their packing in order for them to fit in the single monolayer. We suggest that branching the alkyl tails off the same phenyl ring and the presence of the irregular phenyl rings within the monolayers are limiting factors on the propagation of the positional ordering of the peripheral alkyl tails.

Rod scans of selected diffraction maxima confirm the conclusion about different orientations of the alkyl tails for different compounds. Rod scans and corresponding fit for all three diffraction peaks **AD12-1** have been previously dis-

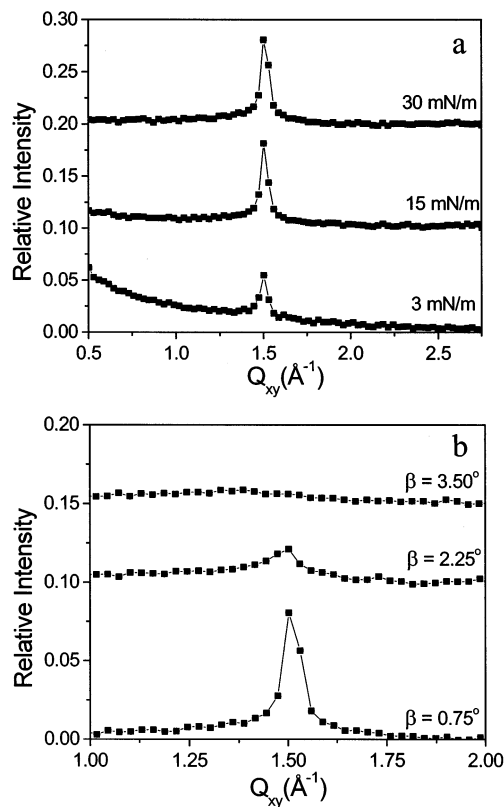


**Figure 6.** Diffraction patterns of **AD12-8** for (a) the whole observed range of  $Q_{xy}$  at three surface pressures, and (b) the high-resolution scans upon increasing the detector away from the horizon ( $\beta$ ). The original intensities are offset for clarity.

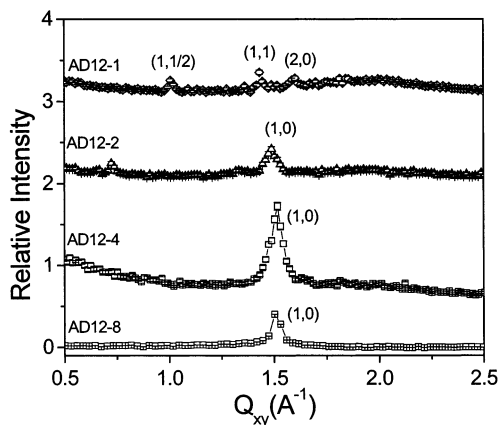


**Figure 7.** Comparison of the observed diffraction patterns of the all dendrimer compounds at the highest surface pressure. The original intensities are offset for clarity.

cussed.<sup>14</sup> The (1,0) peak for the two-tail compound indicates the tails are tilted four degrees in the NN direction. The two lower  $Q$  value peaks for **AD1** to **2-2** were excluded from the rod scan analysis since they could not be indexed properly and the lower intensity of the peaks limited accuracy of the rod scans. The results for the (1,0) peaks for higher generations show the tails tilted insignificantly, only three to four degrees from the surface normal. Representative data for rod scans and the corresponding fits for each sample are shown in Figure 9, and the tilting angles obtained from these fits are presented in Table 1. The results show that tails are in virtually standing-off position for all compounds with multiple tails and the single-tail compound has a tilt angle as high as  $58^\circ$ .

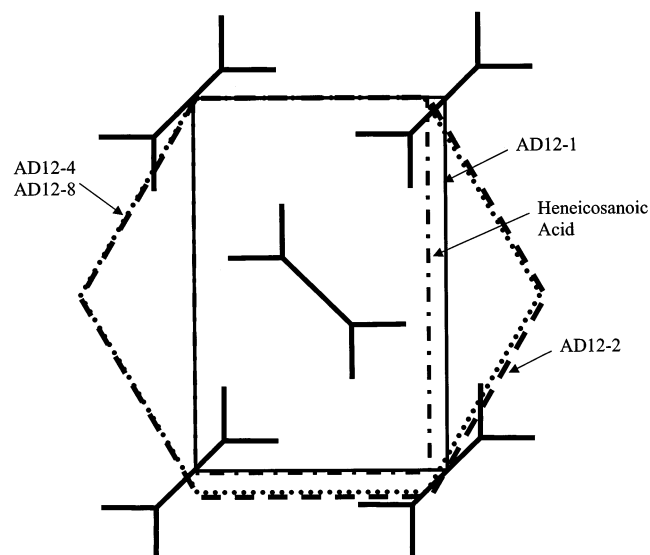


**Figure 8.** The unit cells of **AD12-1** (solid line, half of supercell), **AD12-2** (dashed line), **AD12-4** and **AD12-8** (dotted line) obtained in this work in comparison with the unit cell for alkyl tails (heneicosanoic acid<sup>7</sup>) (dash dotted line).

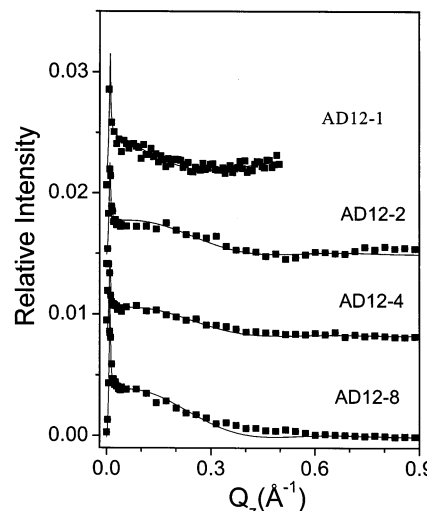


**Figure 9.** Representative rod scans for the main diffraction peaks at the highest pressure labeled with a sample name. Solid lines are the best fits. The intensities were offset for clarity.

**X-ray Reflectivity Studies.** Reflectivity data provides complimentary information on the packing of molecules at the air/water interface by revealing electron density distribution along the surface normal. Figure 10 shows the reflectivity data and the corresponding fits for **AD12-1** and **AD12-8** at the highest pressures, which is representative of all **AD12** compounds. The lower three generations can be fit using two box models at all pressures (Table 2). The eight-tail molecule was fit better using a three-box model. All compounds have total lengths for the molecules at the air/water interface lower than estimated from extended conformation in standing orientation that is consistent with molecule tilting and conformational disorder of the molecular fragments. The monolayers show lower densities as compared to electron density for densely packed tails is  $0.33 \text{ e}/\text{\AA}^3$  that indicates defective monolayer structure in the form, e.g., of clustering within the monolayer.

We observed a level of hydration of the molecules studied by estimating the total number of electrons present in the box models. The total number of electrons per unit cell can be estimated from:  $N_{\text{REF}} = A \int \rho(z) dz$ , where  $A$  is the molecular

**TABLE 2: Fitting Parameters from the Box Models Used to Fit the Reflectivity Data for All Four Compounds at the Highest Pressure<sup>a</sup>**

	AD12-1	AD12-2	AD12-4	AD12-8	uncertainties
head length (Å)	12.9	16	21.1	9.9	±3.0
head density (e/Å <sup>3</sup> )	0.41	0.40	0.38	0.39	±0.02
first tail box length (Å)				13.6	±3.5
first tail box density (e/Å <sup>3</sup> )				0.34	±0.03
second tail box length (Å)	7.5	11.5	11.3	8.2	±2.0
second tail box density (e/Å <sup>3</sup> )	0.24	0.28	0.28	0.10	±0.04
total length (Å)	20.4	27.5	32.4	31.7	
fully extended length (Å)	35	37	43	48	
roughness <sup>a</sup> (Å)	2.7	4.7	3.8	3.4	±0.3

<sup>a</sup> Roughness is for all transitions between the elements of the fitting model. Taken as an identical parameter for all interfaces.

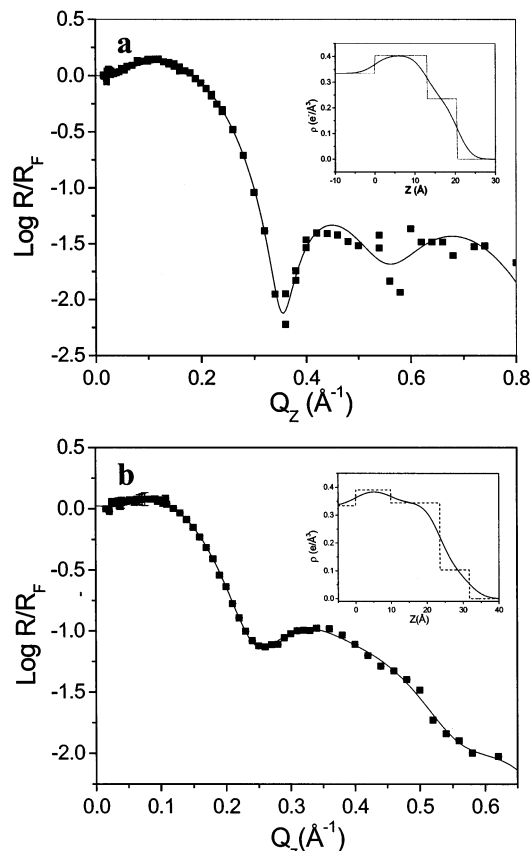


**Figure 10.** X-ray reflectivity and corresponding density distribution models for Langmuir monolayers from (a) AD12-1 and (b) AD12-8. Solid lines represent the best fit. Box models and smeared electron density distributions are shown in insets.

area extracted from the  $\pi$ -A isotherm. Table 2 shows the lengths and densities of the box models for all molecules at the highest pressure along with the calculated roughness and error in the measurements. The higher than expected electron density for the polar head gives rise to the idea of water inclusion in the polar head box, creating a hydration sphere. However, the statistical uncertainty does not allow for calculation of the total number of water molecules included in the present models.

All generations show a trend of the polar head and azobenzene spacer group adapting a tilted behavior beneath the water surface. For the first three compounds, the tilt angle is close to 50° from the surface normal but increases to 63° for AD12-8. The lower than expected thickness of the box model cannot be completely explained by the tilted structure of the molecular fragments or the calculated errors in the model. The effective thickness measured by X-ray reflectivity is averaged over the entire sample area and is not an absolute measurement of the monomolecular film. Therefore, a heterogeneous film structure

with domains is suggested with a lower effective thickness than a complete film. Indeed, domain surface morphology has been observed for monolayers transferred on a solid substrate.<sup>12,13</sup>

**Molecular Packing.** Here we discuss models of molecular packing for all compounds considering all experimental data acquired (Figure 11). First, we observed that the peripheral tails of a single-tail molecule AD12-1 are highly tilted with an approximate tilting angle of 58° from the surface normal. The origin for this tilt came from the large cross-sectional mismatch between the bulky polar head and the single alkyl tail. In contrast, for molecules with multiple tails, the rod scans show minuscule tilts from the surface normal and thereby substantiates the conclusion made from the X-ray diffraction data on the standing tails. The rod scans and the diffraction patterns agree that the tails for the higher generations are orientated along the surface normal, but the box model gives a smaller tail length due to, probably, the fact that the first several carbon atoms of the tails are submerged in the water subphase (Figure 11).

We suggest that the origin of the second tail box in the three-box model for molecule AD12-8 arises from the staggering of the peripheral tails. Rod scans and diffraction data indicate the tails are oriented along the surface normal but each tail is tethered to a phenyl ring that has another alkyl tail attached (Figure 1). The nature of the branching structure hinders the close packing of the tails without reorganization in the molecular structure as was tested on molecular models. The larger phenyl rings at different branching points have to adjust to the space constraints as the tails try to organize in the unit cell. The first and second carbon atoms of the alkyl tails are closely associated with the phenyl ring branching structure. The tilt angle originates at this site, thereby forcing the carbon atoms to be partially associated with the headgroup. The standing-off tails probably begin around the third carbon of the alkyl tail, thereby explaining the short box that correlates with the tails. For all molecules, the head and azobenzene box was considerably shorter than expected, leading to the suggestion that the group is tilted significantly away from the surface normal forming “kink” configuration (Figure 11). Taking the arccosine of the measured length divided by the molecular model length of the group, an angle of 48° to 51° for the first three generations was calculated while the angle was increased for the highest generation to 63°. All models show the headgroups fully submerged in the subphase, but exact arrangement of the polar crown heads could not be deduced from the data collected.

All amphiphilic monodendrons with peripheral alkyl tails form ordered intralayer packing at the air/water interface. AD12-1 packs in a supercell orthorhombic unit cell despite the irregularly large tilt angle of the alkyl tails. The AD12-2 packs in a hexagonal unit cell with additional lower  $Q$  peaks, suggesting a mixed structure but with tails oriented along the surface normal. AD12-4 and AD12-8 also form a hexagonal

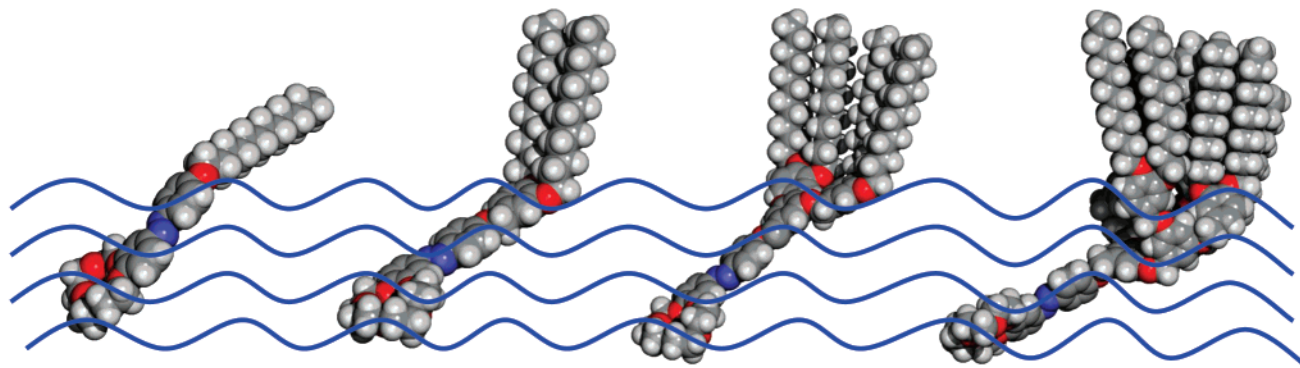


**Figure 11.** Molecular models of AD12-1, AD12-2, AD12-4, and AD12-8 molecules (from left to right) at the air/water interface illustrating the molecular conformation and orientation of different fragments suggested.

lattice. The three highest generations display clear upright orientation of alkyl tails. X-ray reflectivity data indicate the head and azobenzene groups packed in a tilted formation below the water surface for all four compounds, with the highest generation molecule having the largest degree of tilt. The highest generation appears to pack in a stagger pattern due to steric limitations placed on the tails.

We should note that we have not observed any indications of a phase transition from flat-on to stand-off arrangement of hydrophobic tails at different surface pressures. Rather, at low surface pressure (“gas phase”) we observed no indications of molecular ordering with ordered monolayer forming only at high surface pressure. We attribute this behavior to the chemical architectures of monodendron molecules with hydrophobic tails attached to the crown polar head at a single point. Indeed, this architecture does not provide for the driving forces, which can act in favor of flat-on orientation of crown heads as was suggested for several crown-containing amphiphilicities.<sup>10</sup> Instead, “kink” structure is formed with polar head with azobenzene spacer being submerged in water in tilted conformation (Figure 11).

Similarly, no flat-on orientation of the polar crown heads was observed for monodendrons studied recently by Pao et al.<sup>11</sup> The authors varied the number of branches (up to 9 peripheral tails) and the distance of the tails from the branching point and analyzed the density distribution along the surface normal. The smallest cross-sectional mismatch studied in this work was close to 2:1. The model presented in ref 11 showed the alkyl tails extended from the water surface with rodlike behavior while the branching and polar groups extend into the water at an angle away from the surface normal. The presence of large voids between the domains of the tails on a single molecule was also suggested. The area per peripheral alkyl tail determined from  $\pi$ -A isotherms was significantly larger than that expected for a single alkyl chain (26–36 Å<sup>2</sup>) and was attributed to the presence of the bulky phenyl rings. This is in contrast with our studies with cross-sectional area per tails reaching 20 Å<sup>2</sup> despite the phenyl rings presence and indicates a truly ordered state of the peripheral tails despite their branching.

We suggest that the presence of the long spacer (azobenzene group) between the polar head and the peripheral groups is instrumental in the ability of low-generation amphiphilic monodendrons to form ordered intramonomolayer organization. A common structure for multi-tails molecules is hexagonal packing of standing-off alkyl chains and with correlation length close to 40 Å. To adopt this dense packing under constraints imposed by the polar heads and chemical branching, a significant portion of the molecules is submerged in the water subphase forming a “kink” configuration while standing tails adapting staggered

arrangement to fulfill constraints imposed by the chemical attachment to different branching points.

**Acknowledgment.** The authors thank M. Lemieux, M. Ornatska, S. Peleshanko, N. Stephenson, and Dr. M. Lee for technical assistance during experiments. Funding from the National Science Foundation, DMR-0074241, is gratefully acknowledged. The Midwest Universities Collaborative Access Team (MUCAT) sector at the APS is supported by the U.S. Department of Energy, Basic Energy Sciences, Office of Science, through Ames Laboratory under Contract No. W-7405-Eng-82. Use of the Advanced Photon Source was supported by the U.S. Department of Energy, Basic Energy Sciences, Office of Science, under Contract No. W-31-109-Eng-38.

## References and Notes

- (1) Percec, V.; Cho, W.-D.; Mosier, P. E.; Ungar, G.; Yeardley, D. J. *J. Am. Chem. Soc.* **2001**, *123*, 1302. (b) Percec, V.; Cho, W.-D.; Mosier, P. E.; Ungar, G.; Yeardley, D. J. *J. Am. Chem. Soc.* **1998**, *120*, 11061.
- (c) Grayson, Scott M.; Frechet, Jean M. *J. Chem. Rev.* **2001**, *101*, 3819.
- (d) Dykes, Graham M. *J. Chem. Technol. Biotechnol.* **2001**, *76*, 903. (e) Percec, V.; Cho, W. D.; Ungar, G. *J. Am. Chem. Soc.* **2000**, *122*, 10273.
- (2) Balagurusamy, V. S. K.; Ungar, G.; Percec, V.; Johansson, G. *J. Am. Chem. Soc.* **1997**, *119*, 1539. (b) Frechet, J. M. *Science* **1994**, *263*, 5154; *1710*. (c) Newkome, G. R.; Moorefield, C. N.; Vogtle, F. (Ed.) *Dendritic Molecules*; VCH: Weinheim, 1996.
- (3) Tully, D. C.; Frechet, J. M. *J. Chem. Commun.* **2001**, 1229. (b) Kampf, J. P.; Frank, C. W.; Malmstrom, E.; Hawker, C. J. *Langmuir* **1999**, *15*, 227. Saville, P. M.; Reynolds, P. A.; White, J. W.; Hawker, C. J.; Frechet, J. M.; Wooley, K. L.; Penfold, J.; Webster, J. R. *J. Chem. Phys.* **1995**, *99*, 8283.
- (4) Kaganer, V. M.; Brezesinski, G.; Mohwald, H.; Howes, P. B.; Kjaer, K. *Phys. Rev. E* **1999**, *59*, 2141. (b) Kaganer, V. M.; Osipov, M. A. *J. Chem. Phys.* **1998**, *109*, 2600. (c) Brezesinski, G.; Kaganer, V. M.; Mohwald, H.; Howes, P. B. *J. Chem. Phys.* **1998**, *109*, 2006.
- (5) Mindyuk, O. Y.; Heiney, P. A. *Adv. Mater.* **1999**, *11*, 341. (b) Mindyuk, O. Y.; Stetzer, M. R.; Heiney, P. A.; Nelson, J. C.; Moore, J. S. *Adv. Mater.* **1998**, *10*, 1363. (c) Heiney, P. A.; Stetzer, M. R.; Mindyuk, O. Y.; DiMasi, E.; McGhie, A. R.; Liu, H.; Smith, A. B. *J. Phys. Chem. B* **1999**, *103*, 6206. (d) Gidalevitz, D.; Mindyuk, O. K.; Stetzer, M. R.; Heiney, P. A.; Kurnaz, M. L.; Schwartz, D. K.; Ocko, B. M.; McCauley, J. P.; Smith, A. B. *J. Phys. Chem. B* **1998**, *102*, 6688.
- (6) Weidemann, G.; Brezesinski, G.; Vollhardt, D.; Mohwald, H. *Langmuir* **1998**, *14*, 6485.
- (7) Kaganer, V. M.; Mohwald, H.; Dutta, P. *Rev. Mod. Phys.* **1999**, *71*, 779.
- (8) Peterson, I. R.; Russell, G. L.; Earls, J. D.; Girling I. R. *Thin Solid Films* **1988**, *161*, 325.
- (9) Steitz, R.; Peng, J. B.; Peterson, I. R.; Gentle, I. R.; Kenn, R. M.; Goldmann, M.; Barnes, G. T. *Langmuir* **1998**, *14*, 7245.
- (10) Zhu, Y. M.; Jia, X. B.; Xiao, D.; Lu, Z. H.; Wei, Y.; Wu, Z. H.; Hu, Z. L.; Xie, M. G. *Phys. Lett.* **1994**, *188*, 287. Zhu, Y. M.; Wei, Y. *J. Chem. Phys.* **1994**, *101*, 10023. Zhu, Y. M.; Lu, Z. H.; Wei, Y. *Phys. Rev. E* **1995**, *51*, 418. Zhu, Y. M.; Lu, Z. H.; Jia, X. B.; Wei, Q. H.; Xiao, D.; Wei, Y.; Wu, Z. H.; Hu, Z. L.; Xie, M. G. *Phys. Rev. Lett.* **1994**, *72*, 2573.
- (11) Pao, W.; Stetzer, M. R.; Heiney, P. A.; Cho, W.; Percec, V. *J. Phys. Chem. B* **2001**, *105*, 2170.

- (12) Peleshanko, S.; Sidorenko, A.; Larson, K.; Villavicencio, O.; Ornatska, M.; McGrath, D. V.; Tsukruk, V. V. *Thin Solid Films* **2002**, *406*, 233.
- (13) Sidorenko, A.; Houphouet-Boigny, C.; Villavicencio, O.; McGrath, D. V.; Tsukruk, V. V. *Langmuir* **2000**, *16*, 10569.
- (14) Larson, K.; Vaknin, D.; Villavicencio, O.; McGrath, D.; Tsukruk, V. V. *J. Phys. Chem. B* **2002**, *106*, 7246.
- (15) Hashemzadeh, M.; McGrath, D. V. *Prepr. Pap.—Am. Chem. Soc., Polym.* **1998**, *39*, 338.
- (16) Bohm, C.; Leveiller, F.; Jacquemain, D.; Mohwald, H.; Kjaer, K.; Als-Nielsen, J.; Weissbuch, I.; Leiserowitz, L. *Langmuir* **1994**, *10*, 830.
- (17) Weissbuch, I.; Leveiller, F.; Jacquemain, D.; Kjaer, K.; Als-Nielsen, J.; Leiserowitz, L. *J. Phys. Chem.* **1993**, *97*, 12858.
- (18) Vaknin, D.; Kelley, M. S. *Biophys. J.* **2000**, *79*, 2616.
- (19) Vankin, D. In *Methods of Materials Research*; Kaufmann, E. N., Abbaschian, R., Barnes, P. A., Bocarsly, A. B., Chien, C. L., Doyle, B. L., Fultz, B., Leibowitz, L., Mason, T., Sanchez, J. M., Eds.; John Wiley & Sons: New York, 2001; p 10d.2.1.
- (20) Gregory, B. W.; Vaknin, D.; Gray, J. D.; Ocko, B. M.; Stroeve, P.; Cotton, T. M.; Struve, W. S. *J. Phys. Chem. B* **1997**, *101*, 2006.
- (21) Hosemann, R.; Bagchi, S. N. *Direct Analysis of Diffraction by Matter*; Interscience: New York, 1962.
- (22) Kaganer, V. M.; Osipov, M. A.; Peterson, I. R. *J. Chem. Phys.* **1993**, *98*, 3512.
- (23) Peterson, I. R.; Brezesinski, G.; Struth, B.; Scalas, E. *J. Phys. Chem. B* **1998**, *102*, 9437